Int J Adv Manuf Technol (2011) 55:75–81
DOI 10.1007/s00170-010-3045-0

ORIGINAL ARTICLE

Kernel TIF method for effective material removal control in rotating pitch tool-based optical figuring

Hyun-Su Yi · Ho-Soon Yang · Yun-Woo Lee · Sug-Whan Kim

Received: 30 July 2010 / Accepted: 16 November 2010 / Published online: 4 December 2010

Abstract While opticians have used pitch tools for superb surface finishing, their poor controllability in material removal and associated lengthy tooling overhead have been well known in optics fabrication communities. We report a new computational technique called kernel tool influence function (KTIF) that can bring higher predictability to pitch tool-based material removal. The term "kernel" is defined as the ratio of experimental to simulated removal depth, therefore transforming the material removal coefficient of Preston's equation to a removal scaling function at each point on the tool surface. This approach offers a unique inherent control feature incorporating "real-life shop floor effects associated with pitch tool polishing variables" into the tool influence functions without the need for theoretical expressions for the effects of individual variables on material removal behavior. Using a modified Draper-type polishing machine and a rotating pitch tool, we first generated kernel TIFs with zero stroke and used them for simulation and trial experiments of extended TIFs with variable tool strokes. The results show that the root mean square (rms) TIF profile differences between the prediction and experiments are in the range of 11 to 29 nm for conventional TIF and 7 to 15 nm for the KTIF. We then generated conventional TIF and KTIF database sets and applied them to surface figuring simulations. The results confirm that the kernel TIF has superior performance to the conventional TIF in controlling the material removal for correction of the chosen surface error.

Keywords Tool influence function · Polishing · Figuring · Pitch

Abbreviations

TIF	Tool influence function
KTIF	Kernel tool influence function
NCTIF	Normalized conventional tool influence function
NKTIF	Normalized kernel tool influence function

1 Introduction

Computerized numerical control (CNC)-based optical surfacing techniques have been evolving rapidly since the 1980s. Examples include the Canon super-smooth polisher (CSSP) [1–3], stressed lap polishing [4, 5], ion beam finishing [6], "precession" processes [7–9], and magneto-rheological finishing (MRF) [10–12]. These techniques have been successfully used to produce high-quality optical surfaces. For example, a CSSP aided by on-machine coordinate measuring systems and pitch tools on the flexible layer was used to achieve a surface roughness of

H.-S. Yi
Department of Measurement Science,
University of Science and Technology,
113 Gwahangno, Yuseong,
Daejeon 305-333, South Korea

H.-S. Yi · H.-S. Yang · Y.-W. Lee
Center for Space Optics,
Korea Research Institute of Standards and Science,
P.O. Box 102, Yuseong,
Daejeon 305-600, South Korea

S.-W. Kim (✉)
Space Optics Laboratory, Department of Astronomy,
Yonsei University,
134 Sinchon-dong, Seodaemun-Gu,
Seoul 120-749, South Korea
e-mail: skim@csa.yonsei.ac.kr

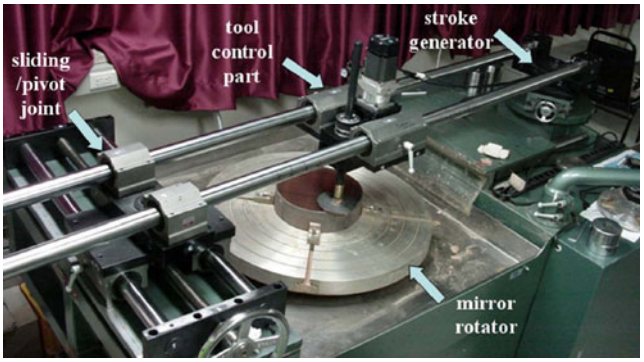

Fig. 1 Modified Draper-type polishing machine

less than 0.2 nm root mean square (rms) for fused silica and SiC mirrors [1]. Ion beam figuring techniques, while they suffer from low material removal rates, were used to produce the 1.8-m hexagonal mirror segments for the Keck telescope primary mirror [6]. Stressed lap polishing techniques have demonstrated their efficiency and controllability in polishing and figuring processes for large mirrors ranging from ≈1 to ≈8.4 m in diameter [4, 5]. "Precession" processes (Zeeko) and MRF (QED) are representatives of commercialized CNC polishing techniques for optical components up to ~500 mm in size [8, 13, 14]. These modern optics polishing techniques have overcome several problems associated with traditional polishing, such as estimation of time required, low automation rates, and difficulty of technique conservation [14].

Concurrent with these technical developments, various surfacing materials such as polyurethane [8, 15, 16], synthetic cloth [15, 17], and pitches [1, 18] have been used as tool surfaces. Among them, pitch has been perhaps one of the most widely used materials in optics fabrication shops for its characteristic of generating smooth surfaces. Earlier studies include an optical glass (BK7) polished to 0.53 nm rms in surface roughness [19] and fused silica polished to ~0.035 nm rms in surface roughness [1]. However, because it is a "stiff" but highly viscous material [18, 19], pitch has low controllability and requires high tooling overhead, contributing to low process convergence. Therefore, many opticians recognize that pitch-based deterministic and/or CNC-based process control is extremely difficult and challenging, if not impossible.

Earlier studies on the material removal characteristics of pitch tools in relation to optics fabrication include Jones [18, 20] and Donald et al. [21]. While their investigations were focused on developing a figuring algorithm and automated polishing process with the emphasis on final surface profile correction, their studies revealed good agreement between prediction and experiment in material removal. However, at the time of writing, we acknowledge that the systematic investigation of material removal predictability and/or controllability for the rotating pitch tool has received relatively little attention from the optics fabrication community.

Addressing this, we have explored a new computational technique called kernel tool influence function (KTIF) to improve the prediction accuracy in optical material removal with rotating pitch tools. In Section 2, we describe the experimental apparatus, a modified Draper-type polishing machine, derive the rotating tool motion equation, and present the initial material removal experiment results in TIF generation. In Section 3, we suggest the new concept of KTIF. This is followed by prediction of its material removal performance, which is demonstrated from trial experiments in Section 4. In

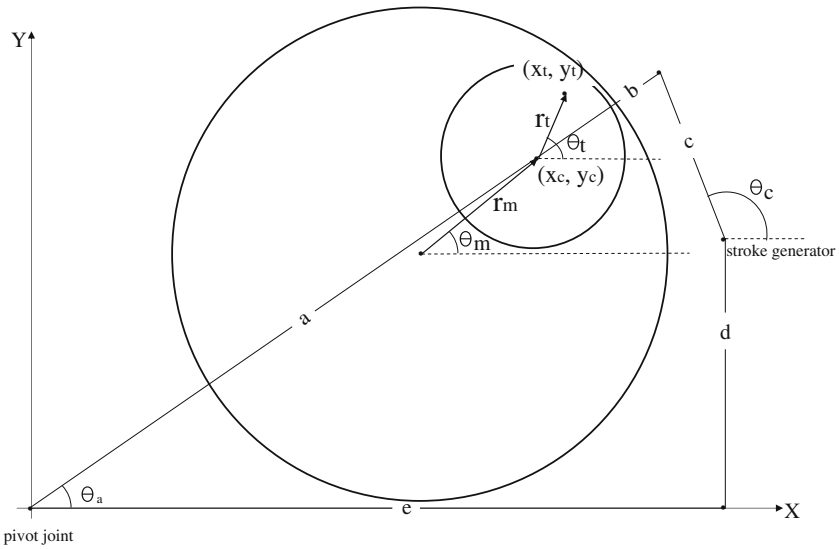

Fig. 2 Machine configuration for tool motion analysis and TIF generation computation

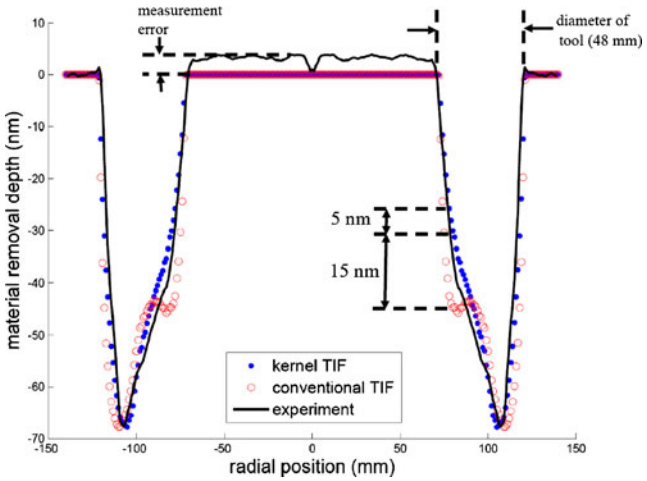

Fig. 3 Simulated and experimental removal depth profiles when the workpiece is rotated and the rotating tool is positioned off-center

Section 5, we show the simulated figuring performance of KTIF versus conventional TIF. Implications and concluding remarks are offered in Section 6.

2 Conventional TIF for a Draper-type polishing machine

The tool influence function (TIF) can be defined as the tool material removal footprint on an optical surface over the duration of the rubbing time; hence, it is closely related to the machine characteristics that influence the polishing variables, including rubbing pressure, relative velocity between tool and workpiece surface, and time. For this study, we used a modified Draper-type machine as shown in Fig. 1. It consists of four major subsystems: workpiece rotator, rotating polishing tool, stroke generator, and sliding/pivot joint. The tool motion on the rotating workpiece surface is controlled by adjusting the length and rotation speed of the stroke arm. The pivot joint on the motorized motion sliding rail provides a fixed reference point for the intended tool motion on the workpiece surface. This configuration enables efficient tool motion control translating three rotation motions (i.e., workpiece, tool, and stroke arm rotator) into controllable tool motion trajectories for a wide variety of TIF generation.

The conventional TIF can be obtained from straightforward application of the well-known Preston equation:

$$\Delta z_{\mathrm{con}} = \kappa \cdot P \cdot V \cdot \Delta T, \tag{1}$$

where Δz_{con}, κ, P, V, and ΔT are the material removal depth, removal coefficient, polishing pressure, relative speed of the tool on the workpiece, and dwell time, respectively. Computing Eq. 1 requires prior knowledge of the tool trajectory; Fig. 2 shows the machine configuration variables used to determine the tool trajectory. In this figure, a is the distance between the pivot joint and the tool center, b is the distance between the tool center and the stroke arm, c is the length of the stroke arm, d is the shortest distance between the stroke generator and the machine's Y-axis, and

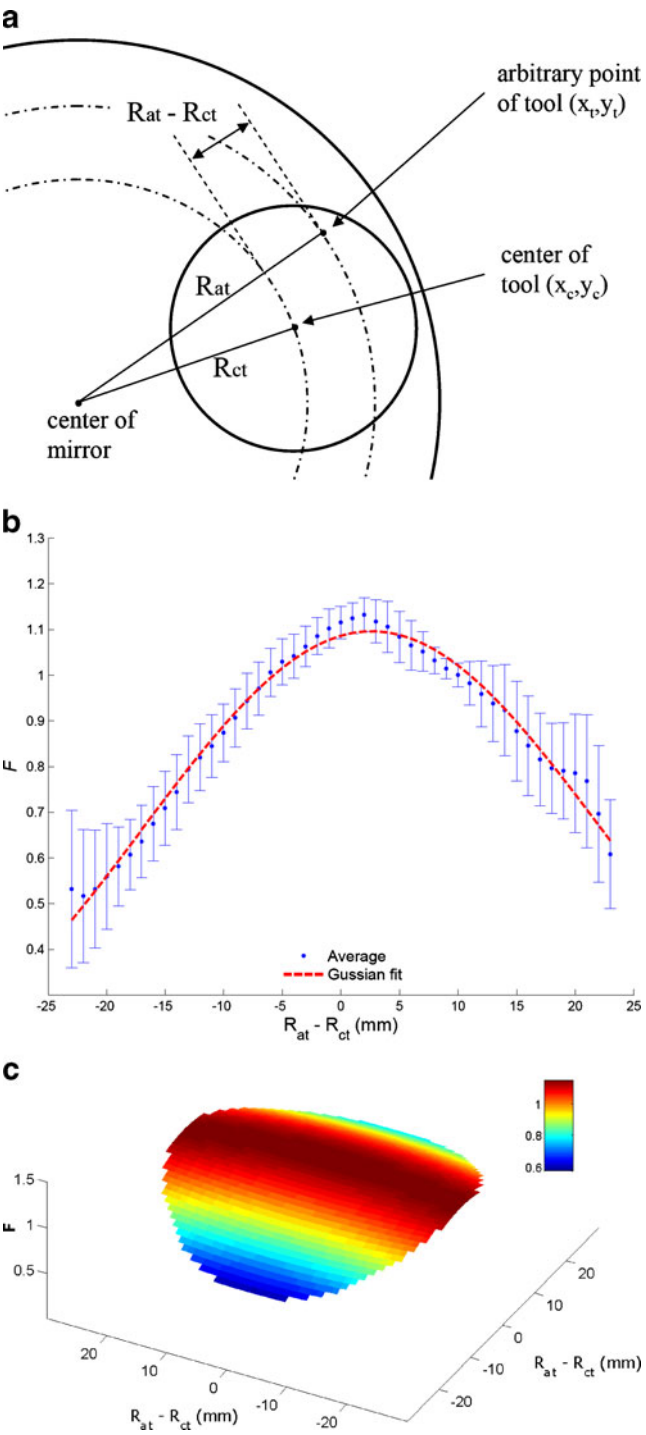

Fig. 4 **a** Schematic diagram related to kernel shape parameters; **b** 2D plot of averaged kernels from four figuring experiments; **c** 3D plot of averaged kernels across the tool

Table 1 Various figuring conditions with diverse motions of tool

Case	Tool sweep length (mm, max. 300)	Stroke (mm)	Radial distance of tool center (mm)	Polishing time (min)
1	190	30	109	144
2	220	50	100	50
3	256	90	115	64

e is the shortest distance between the stroke generator and the machine's X-axis. We can then express the TIF as:

$$\Delta z_{\text{con}}(x_t, y_t; x_c, y_c) = \kappa \cdot W_{\text{tool}}/A_{\text{contact}} \cdot \left(V_x^2 + V_y^2\right)^{1/2} \cdot \Delta T, \quad (2)$$

where $V_x = -\dot{\theta}_m(r_m \cos\theta_m + r_t \cos\theta_t) + \dot{\theta}_t r_t \cos\theta_t + \dot{a}\cos\theta_a - a \cdot \dot{\theta}_a \sin\theta_a$, $V_y = -\dot{\theta}_m(r_m \sin\theta_m + r_t \sin\theta_t) + \dot{\theta}_t r_t \sin\theta_t + \dot{a}\sin\theta_a + a \cdot \dot{\theta}_a \cos\theta_a$.

Here, W_{tool} is the total tool weight and A_{contact} is the contact area between the tool and workpiece surface, and θ_m, θ_t, and θ_a are the rotational velocities of the mirror, tool, and pivot joint, respectively.

To check the performance of Eq. 2, we ran a trial polishing run and compared the experimental removal depth profile with that of the theoretical TIF computed from Eq. 2. For this experiment, the tool rotated at 100 rpm on the workpiece with no stroke for 20 min. The workpiece rotation was set to 6 rpm. The tool center was positioned 100 mm from the center of the workpiece. The pitch lap was about 48 mm in diameter and the resulting polishing pressure was 0.0184 N/mm^2. The workpiece was an Astro-Sitall mirror blank of 300 mm in diameter and its surface was prepared to the nominal form accuracy of 0.5 μm p-to-v (peak to valley).

The measured removal profile and conventional TIF are depicted in Fig. 3. We note that the two curves are well matched to each other in general; however, a profile mismatch becomes prominent at around ±75 mm in radial position, where it has the maximum profile difference of around 15 nm (i.e., 22% of the maximum removal depth of 68 nm). Such discrepancies could accumulate to an unacceptable level if the experiment run was made for longer, or if an actual form correction figuring run was made with various tool trajectories. Therefore, we should devise a better computation method for improved TIF prediction accuracy.

3 Generation of kernel TIF

Several parameters, such as the material properties of the pitch, slurry density, fluid pressure, and/or stress distribution [22, 23], can influence the predictability of material removal in the optical surfacing process. We recognize that incorporating effects of these parameters into Preston's removal coefficient (κ) is impractical for the generation of a realistic TIF, as each variable has highly nonlinear and complex relationships with material removal. For these reasons, we define "kernel" as the ratio of experimental to simulated removal depth at each point on the tool. The kernel TIF (KTIF) can be expressed as in Eq. 3, where F defines "kernel." We note that the concept of "kernel F" is different from the standard material removal coefficient κ of Preston's Eq. 1. While "fixed constant κ" is applied for the whole area of tool–optical surface contact, "kernel F" varies across the contact area during the machine run as it takes into account the effects of nonuniformity and the instability of all variables.

$$\Delta z_{\text{ker}}(x_t, y_t; x_c, y_c) = F(x_t, y_t; x_c, y_c) \cdot \Delta z_{\text{con}}(x_t, y_t; x_c, y_c) \quad (3)$$

A trial material removal experiment was carried out with a rotating tool positioned at around 100 mm away from the center of the rotating workpiece. The other experimental conditions were the same as in Section 2, except for zero stroke motion. Because the tool revolves around the center of the workpiece surface, F becomes a function of the relative radial position of the polishing tool on the workpiece: (R_{at}–R_{ct}). Figure 4a shows the experimental configuration and the resulting kernels averaged over four measurements are shown in Fig. 4b and c. The dots and bars in Fig. 4b show the averaged value and standard deviation of the kernel Fs. For practical usage of F, it can be fitted to a Gaussian function as follows:

$$F(x_t, y_t; x_c, y_c) = a \cdot e^{-\left(\frac{R_{at} - R_{ct} - b}{c}\right)^2} \quad (4)$$

Here, a least-square-fitted a is 1.096 and b is 2.64 mm, while c is 27.66 mm and R^2 (coefficient of determination) is 0.9832. Because the peak point deviates 2.64 mm away from the tool center, the kernel F has asymmetric variation, as appeared in Fig. 4b and c. We can now argue: (1) that the standard Preston's interpretation of material removal is a subset of the polishing regime in which F=1; and (2) that there may exist a wider variety of polishing regimes where F≠1. When applying this fitted kernel function (4), we find (1) that the simulated KTIF produces 5 nm n the maximum removal profile difference whereas the conventional TIF results in 15 nm at the radial position of ±75 mm; and (2) that the simulated KTIF yields 3 nm in rms profile difference, whereas the conventional TIF exhibits 7 nm, as shown in Fig. 3.

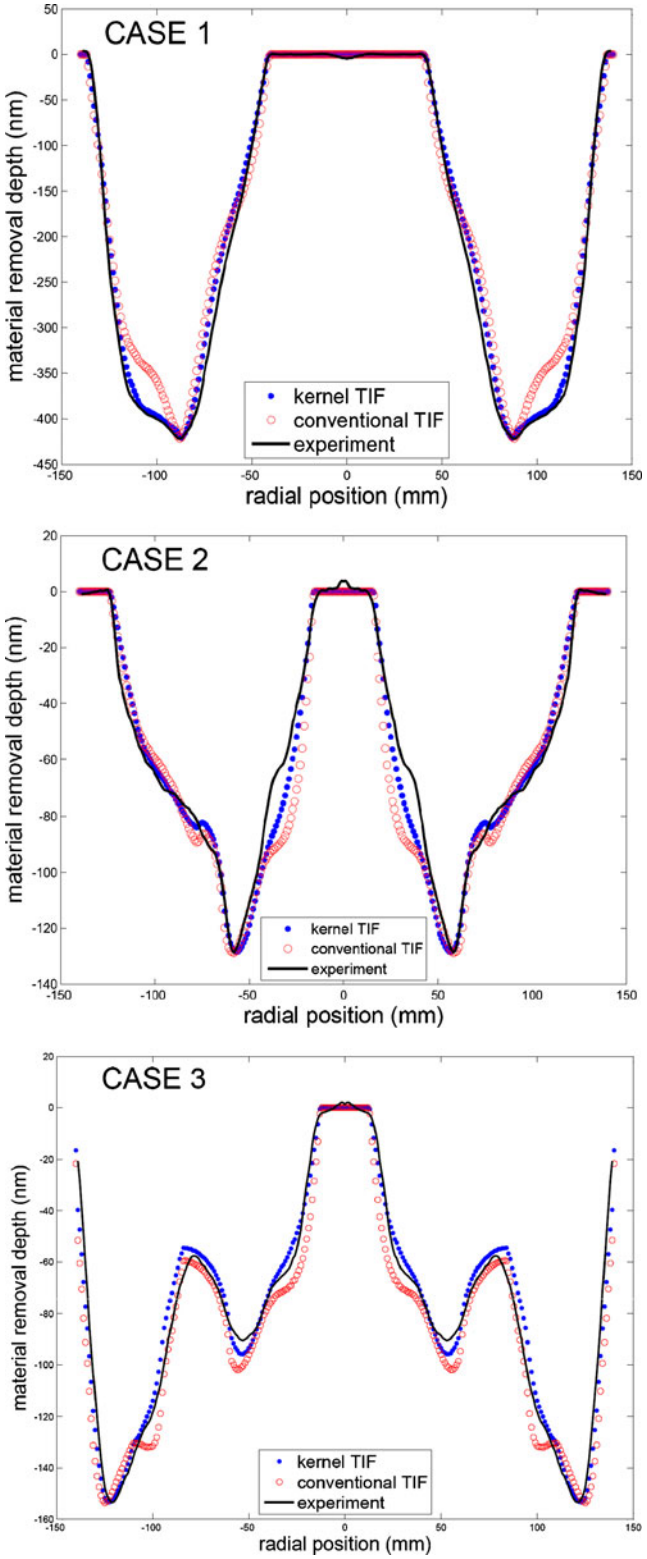

Fig. 5 Various material removal shapes for three different tool motions

4 KTIF performance

We ran three material removal experiments, simulating surfacing figuring to a limited extent. The experimental input conditions are listed in Table 1, assuring diverse tool motions on the workpiece. The same tool and workpiece as the previous KTIF generation experiment with zero stroke were used. We note that, as the stroke parameter increases, the tool motion becomes more complex and the material removal area on the workpiece surface also increases. For this reason, the sweeping width on the mirror surface varied from 190 to 256 mm, to check whether the KTIF with zero stroke maintained its high prediction accuracy with an increase in rubbing area. Other than the three input conditions listed in Table 1, the remaining input polishing conditions were identical to those in the experiment described in Section 2.

The experimental results (black solid line) and predicted removal shapes from using KTIF (blue solid circles) and conventional TIF (red open circles) are shown in Fig. 5. The rms profile differences between the predicted and experimental results are summarized in Table 2. In Table 2, the improvement in prediction error was calculated from the ratio of the difference between the rms profile differences of KTIF and of conventional TIF to the rms profile difference of the conventional TIF. We note that: (1) the KTIF exhibits much better prediction performance than the conventional TIF in all cases; (2) the KTIF prediction performance remains more or less the same while the material removal area increases on the work piece surface; and (3) the profile differences between the predicted and experimental results are most prominent where the surface profile slope changes sharply; interestingly, this is where the prediction performance gain of the KTIF over the conventional TIF is most observable.

However, at this point, one may argue that the rms profile difference from the use of KTIF with 48-mm sweep length (i.e., zero stroke) should worsen as the sweep length is increased with the case number (i.e., Case 1, Case 2, Case 3). In general, this argument seems to be supported with smaller value of the Case 1 than those of Cases 2 and 3 in the removal depth normalized rms profile difference, as shown in the fifth columm of Table 2. At the same time, when we focus onto Case 2 and 3, we see a reversal trend contradicting to the aforementioned argument. We note that, at the time of this writing, the lack of experiment numbers contributes to the current ambiguity in trend analysis and therefore acknowledge the need for further experimental investigation which will be a main scope of the following publication in series. Nevertheless, the results shown in Fig. 5 and Table 2 are clear enough to assert that the KTIF technique is superior to the conventional TIF method in predicting and therefore controlling the material removal with rotating pitch tools.

Table 2 RMS profile difference between experiment and prediction

Case	Conventional TIF (rms)	KTIF (rms)	Conventional TIF (depth normalized to 1 μm, NCTIF, rms)	KTIF (depth normalized to 1 μm, NKTIF, rms)	Improvement in prediction error[a]
1	29 nm	15 nm	69 nm	36 nm	48%
2	11 nm	7 nm	85 nm	54 nm	36%
3	12 nm	7 nm	78 nm	45 nm	42%

[a] Improvement in prediction error=(rms of NCTIF−rms of NKTIF)/rms of NCTIF

5 Simulated figuring performance of KTIF

We also compared the KTIFs and conventional TIFs in a surface figuring simulation. We built two sets of extended TIF databases using KTIFs and conventional TIFs. The first database contains 2,156 conventional TIFs determined by tool position and stroke varied in regular steps. The second database was built with KTIFs derived from the same sets of tool parameters as the conventional TIFs. The workpiece and tool rotational speeds were the same as in the previous section.

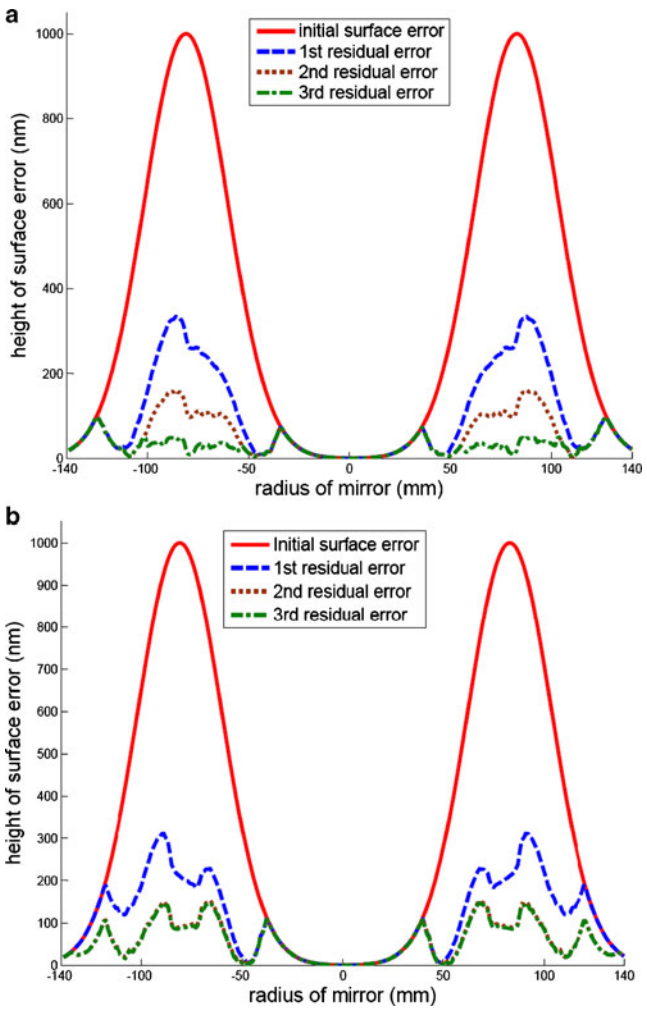

Fig. 6 Simulated figuring results: **a** Residual surface error from KTIF **b** Residual surface error from conventional TIF

The figuring algorithm uses an initial surface error input, and a best-fit extended TIF is then selected. The best-fit TIF is defined as an extended TIF generating the smallest residual surface error in terms of p–v and rms values when the resulting surface is compared with the target surface shape. The control parameters for the TIF used are then stored and the resulting surface map is saved and used as the new surface error input. When the p–v and rms residual surface errors are not improved anymore, the figuring simulation stops.

For the trial figuring simulation, we used a donut-shaped surface error incorporated in the initial surface. It has 1 μm p–v error and 347 nm rms error. A total of three figuring simulations were carried out using each TIF database, and the results are presented in Fig. 6. Once again, the kernel TIF database exhibits better performance: the residual surface profile errors with the kernel TIF database are 101 nm p–v and 21 nm rms errors, while the conventional TIF database gives 157 nm p–v and 41 nm rms errors.

6 Concluding remarks

We have developed a new computational technique called KTIF to increase the predictability of material removal in pitch tool-based surface figuring. As opposed to the conventional TIF computed from the straightforward application of Preston's equation, a KTIF computation technique benefits uniquely from the simple and practical use of integrated material removal effects caused by the instability and nonuniformity of all real-life polishing parameters (such as the properties of the tool material, fluid pressure, and stress distribution) during a polishing run.

In particular, the superior prediction performance of the KTIF over the conventional TIF has been proven in three TIF generation experiments. Furthermore, the three figuring simulations to remove the donut-shaped surface error of 1 μm in p–v shows the superior performance of the KTIF-based material removal control as opposed to that of the conventional TIF-based technique.

We note that earlier studies on TIF were concerned mainly with building precessions tools that used polishing cloths and with the repeatability of TIF generation in view of its associated CNC process control algorithm [7, 24, 25]. On the other hand, this study shows clear benefits of the KTIF technique and its accuracy in predicting the experimental removal profile with rotating pitch tools. This tends to support an increased value for rotating pitch tools that have the potential, even today, for CNC-style optical surfacing toward the "deterministic" polishing and figuring processes in the optics fabrication industry.

Acknowledgments The authors would like to thank Dr. Hyug-Gyo Rhee and Mr. Jae-Hyeob Lee for valuable discussions in this research.

References

1. Ando M, Negishi M, Takimoto M, Deguchi A, Nakamura N, Higomura M, Yamamoto H (1992) Super-smooth surface polishing on aspherical optics. Proc SPIE 1720:22–33
2. Negishi M, Ando M, Takimoto M, Deguchi A, Narumi H, Nakamura N, Yamamoto H (1995) Super-smooth surface polishing on aspherical optics(I) –high-precision coordinate measuring and polishing systems-. Proc SPIE 2576:336–347
3. Ando M, Negishi M, Takimoto M, Deguchi A, Nakamura N (1995) Super-smooth surface polishing on aspherical optics(II): achievement of a super-smooth polishing. Proc SPIE 2576:348–356
4. Martin HM, Burge JH, Miller SM, Smith BK, Zehnder R, Zhao C (2006) Manufacture of a 1.7 m prototype of the GMT primary mirror segments. Proc SPIE 6273:62730G. doi:10.1117/12.672105
5. Martin HM, Allen RG, Cuerden B, Hill JM, Ketelsen DA, Miller SM, Sasian JM, Tuell MT, Warner S (2006) Manufacture of the second 8.4 m primary mirror for the Large Binocular Telescope. Proc SPIE 6273:62730C
6. Allen LN (1995) Progress in ion figuring large optics. Proc SPIE 2428:237–247
7. Walker DD, Brooks D, King A, Freeman R, Morton R, McCavana G, Kim S-W (2003) The 'Precessions' tooling for polishing and figuring flat, spherical and aspheric surfaces. Opt Express 11:958–964
8. Walker DD, Beaucamp ATH, Bingham RG, Brooks D, Freeman R, Kim SW, King A, McCavana G, Morton R, Riley D, Simms J (2003) The precessions process for efficient production of aspheric optics for large telescopes and their instrumentation. Proc SPIE 4842:73–84
9. Walker DD, Beaucamp ATH, Brooks D, Doubrovski V, Cassie M, Dunn C, Freeman R, King A, Libert M, McCavana G, Morton R, Riley D, Simms J (2004) Recent development of precessions polishing for larger components and free-form surfaces. Proc SPIE 5523:281–289
10. Shorey AB, Jacobs SD, Kordonski WI, Gans RF (2001) Experiments and observations regarding the mechanisms of glass removal in magnetorheological finishing. Appl Opt 40:20–33
11. DeGroote JE, Marino AE, Wilson JP, Bishop AL, Lambropoulos JC, Jacobs SD (2007) Removal rate model for magnetorheological finishing of glass. Appl Opt 46:7972–7941
12. Mao C, Shafrir SN, Lambropouls JC, Mici J, Jacobs SD (2009) Shear stress in magnetorheological finishing for glasses. Appl Opt 48:2585–2594
13. Shorey A, Kordonski W, Tricard M (2004) Magnetorheological Finishing of large and lightweight optics. Proc SPIE 5533:99–107
14. Jacobs SD (2004) International innovations in optical finishing. Proc SPIE 5523:264–272
15. Walker DD, Brooks D, Freeman R, King A, McCavana G, Morton R, Riely D, Simmson J (2001) The first aspheric form and texture results from a production machine embodying the precession process. Proc SPIE 4451:267–276
16. Li Y, Hou J, Xu Q, Wang J, Yang W, Guo Y (2008) The characteristics of optics polishied with a polyurethane pad. Opt Express 16:10285–10293
17. Walker DD, Beaucamp ATH, Bingham RG, Brooks D, Freeman R, Kim SW, King A, McCavana G, Morton R, Riley D, Simms J (2003) Precessions aspheric polishing:- new results from the development programme. Proc SPIE 5180:15–28
18. Jones RA (1986) Computer-controlled optical surfacing with orbital tool motion. Opt Eng 25:785–790
19. Leistner AJ, Thwaite EG, Lesha F, Bennett JM (1992) Polishing study using Teflon and Pitch laps to produce flat and supersmooth surfaces. Appl Opt 31:1472–1482
20. Jones RA, Plante RL (1985) Rapid fabrication of large aspheric optics. Proc SPIE 0571:85–91
21. Small DW, Hoskins SJ (1986) An automated aspheric polishing machine. Proc SPIE 645:9
22. Srinivasa-Murthy C, Wang D, Beaudoin SP, Bibby T, Holland K, Cale TS (1997) Stress distribution in chemical mechanical polishing. Thin Solid Films 308–309:533–537
23. Zhou C, Shan L, Hight JR, Ng SH, Danyluk S (2002) Fluid pressure and its effects on chemical mechanical polishing. Wear 253:430–437
24. Kim DW, Kim S-W (2005) Static tool influence function for fabrication simulation of hexagonal mirror segments for extremely large telescopes. Opt Express 13:910–917
25. Kim DW, Park WH, Kim S-W, Burge JH (2009) Parametric modeling of edge effects for polishing tool influence functions. Opt Express 17:10